MSc thesis in Mechanical Engineering

Transport properties of acid gasses in aqueous MDEA solvents

Casper van der Geest

2022

TU Delft

Photo: Corné Sparidaens

MSc thesis in Mechanical Engineering

Transport properties of acid gasses in aqueous MDEA solvents

Casper van der Geest

November 2022

A thesis submitted to the Delft University of Technology in partial fulfillment of the requirements for the degree of Master of Science in Mechanical Engineering

Casper van der Geest: *Transport properties of acid gasses in aqueous MDEA solvents* (2022)

The work in this thesis was carried out in the:

Process & Energy department - 3mE
Delft University of Technology

Supervisors:	Dr. Othon Moultos
	Mert Polat
Assessment committee:	Dr. Poulumi Dey
	Dr. Othon Moultos
	Prof. Thijs Vlugt

Abstract

Acid-gas capture systems are used to remove acid-gasses from waste gas streams from combustion or other chemical processes. A commonly used solvent is an aqueous solution with the primary amine monoethanolamine (MEA). Removing the acid gasses typically involves heating the solvent to approximately 378-383K in the stripping reactor. Using methyldiethanolamine (MDEA) instead of MEA can reduce the heating energy consumption of the stripper due to its lower reaction heat. The design of new reactors using aqueous MDEA solvents requires more data describing the properties of this solvent. Literature reporting thermophysical properties of aqueous MDEA solvents and transport properties of acid gasses in these solvents is exceedingly scarce. This work fills that information gap. Molecular dynamics were employed to compute density, viscosity and diffusivity of MDEA, CO_2 and H_2S in aqueous MDEA ranging in 0-50 wt% MDEA and 288-323K. The simulations were conducted using fully atomistic force fields for all species. The charges of MDEA were computed using Gaussian09 and scaled to achieve optimal agreement with experimental density and viscosity data. It has become clear that N-C-C-O dihedral in MDEA is crucial to reproduce experimental data of the viscosity and the diffusivity of MDEA. Two dihedrals were tested to achieve the best results. The resulting computed density, viscosity and diffusivity of MDEA are in good agreement with experimental data. The mixing rules between MDEA and CO_2 were adjusted to increase accuracy of the prediction of diffusivity of CO_2. The results are in good agreement with experimental data at 0-10wt% MDEA or 288K. The deviations become larger with higher wt% MDEA or higher temperatures.

Contents

1 Introduction

The challenge of climate change requires drastic changes to reduce the effective carbon emissions of many industries[1]. Two major users of fossil fuels are the energy and industrial sectors[2]. The energy sector is primarily made up of plants which burn fossil fuels to generate electricity[2]. The chemical sector will use chemical feed stock, various reactors and large amounts of energy to produce the products required to run the modern world. Some of these processes may produce greenhouse gasses, either as a chemical byproduct or while generating the energy used in the process.

One approach to reducing energy consumption or waste gas emissions involves changes to the existing processes. This is considered unattractive, due to the vast capital investment required for redesigning and rebuilding existing machinery. Another approach is post combustion capture. Post combustion capture systems, as the name suggests, capture greenhouse gasses from existing waste gas streams. This approach offers several advantages, one of which is the ability to retrofit existing plants. This makes post combustion capture an easy approach to reduce the emissions of existing processes[3]. Chemical absorption using aqueous monoethanolamine (MEA) is a popular choice due to its high rate of absorption, low viscosity, high solubility of acid gasses and low cost. A major drawback is the high energy consumption when regenerating the solvent in the stripper[4]. Tertiary amines such as methyldiethanolamine (MDEA) have a lower reaction heat than MEA, which reduces the heating requirement in the regeneration process[5]. The solvent fluid properties are generally obtained experimentally. However, literature describing aqueous MDEA solvents is scarce. As a cost and time saving measure, experimental data can be supplemented by molecular simulations. In this work, molecular dynamics is used to compute the density and bulk viscosity of the system, as well as the diffusivity (D) of MDEA, CO_2 and H_2S; ρ_{bulk}, η_{bulk}, D_{MDEA}, D_{CO_2} and D_{H_2S}.

1.1 Existing literature

Various amines have been studied using molecular simulations to get a better understanding of their behavior in aqueous systems. MEA is a popular choice of amine in acid capture systems[6]. A large amount of research exists describing the behavior of this amine when employed in the acid gas capture process[7][8][9][10]. Some computational work was conducted as well[11][12]. Molecular simulation is a great complement to measuring the diffusivity of acid gasses in this process. Measuring the diffusivity of CO_2 directly is very difficult because both CO_2 and H_2S are very reactive in water[13]. Substituting N_2O for CO_2 is common practice[14][15][16][17]. This N_2O/CO_2 analogy uses the assumption that the solubility ratio between N_2O and CO_2 is equal to the diffusivity ratio. It is important to know whether using CO_2 in simulations instead of N_2O yields the same ratio. Molecular simulations do not simulate reactions. This allows us to test both. The work of Chen et al[18] shows that free N_2O and free CO_2 have very similar

diffusivities when conducting molecular simulations. They report a 2% decrease in self diffusivity when using N_2O instead of CO_2. This is achieved by using TIP4P/2005 for water, TRAPPE for CO_2 and the work of Lachet et al[19] for N_2O. This ratio will change when using different force fields. We will use the same force fields, which means the analogy is not necessary.

The acid gasses are removed from the solvent by heating it in "stripper" reactor. The heating energy required for this process is very high for aqueous MEA solvents[4], which is a major drawback of using MEA. Solvents using tertiary amines have a lower reaction heat than MEA[5]. This reduces the heating energy consumption of the stripper. One of these tertiary amines and the focus of this work is MDEA. Plenty of literature exists reporting the density and viscosity of aqueous MDEA[16][20][21][22]. Computational work describing force fields for MDEA is less common and largely focused on their bulk properties. Orozco [23] used a UAU forcefield for pure MDEA over a range of 600-675K for density and 394-444K for viscosity. Their density was in good agreement with experimental data. Their predicted viscosity overestimated experimental data by approximately 20%. Yu et al[24] reported density and viscosity of a mixture of various fully atomistic amines, including MDEA. However, they only investigated mixtures containing pure or multiple amines. Their results can therefore not be used for aqueous MDEA solvents. Yiannourakou et al[25] studied 30wt% aqueous MDEA using a united atom force field for MDEA. They used molecular dynamics to compute, among others, viscosity and D_{CO_2} over a temperature range of 300-400K. Their reported viscosity was approximately 50% lower than experimental data in this range.

Literature reporting experimental data for D_{CO_2} in aqueous MDEA is exceedingly scarce. Al Ghawas et al[16] reported experimental data of D_{CO_2} in aqueous MDEA over a range of 0-50 wt% MDEA and 288-323K. They used the aforementioned N_2O/CO_2 analogy. However, these temperatures are less convenient in the acid gas application. We are interested in the properties of rich solvent present in the stripper. Stripping reactors commonly run at approximately 378-383K and 150-200 kPa, depending on the solvent[26]. This is outside the range reported by Al Ghawas et al[16]. An alternative to the experimental data from Al Ghawas[16] is the computational data reported by Yiannourakou et al[25]. They computed D_{CO_2} in an aqueous mixture of 30 wt% MDEA over a range of 300-400K. However, they computed only 1 data point within the range of Al Ghawas[16]. The result at this data point exceeded experimental data from Al Ghawas[16] by 80%. No experimental data was found reporting D_{CO_2} in the aforementioned temperature and pressure ranges present in the stripper. This work will therefore be restricted to the conditions used by Al Ghawas[16].

Another commonly addressed acid gas in the industry is H_2S. Solvents with aqueous MDEA have a useful property; their selectivity towards H_2S over other impurities in the gas flow[16]. Despite this, no literature studies were found reporting D_{H_2S} in aqueous MDEA; neither experimentally nor computationally. Some data exists of D_{H_2S} in pure water[27]. This will serve as a comparison. The addition of MDEA to the system lowers D_{CO_2}, and will likely have the same effect on D_{H_2S}.

The purpose of this work is to investigate the transport properties of acid gasses in aqueous MDEA and fill the gap in literature. Furthermore, the force field of MDEA will give improved computational results for bulk properties, primarily viscosity, of aqueous MDEA solvents. The properties obtained in this work will aid in the design of new reactors employing aqueous MDEA solvents.

1.2 Acid gas capture process

The feed gas is brought into contact with the solvent in the absorber, allowing the acid-gasses to dissolve into the solvent. Two reactions will occur; one with CO_2 and one with H_2S.

The reaction with H_2S is the same irrespective of the type of used amine [28]. A proton will separate from H_2S. This proton is subsequently absorbed by MDEA.

$$MDEA_{(l)} + H_2S_{(g)} \rightleftarrows MDEAH^+_{(aq)} + HS^-_{(aq)} \tag{R1}$$

The reaction with CO_2 is slightly more complex. First, CO_2 and H_2O will react to form carbonic acid. This carbonic acid will decompose into bicarbonate and a proton. This proton is then absorbed by MDEA.

$$CO_{2(g)} + H_2O_{(l)} \rightleftarrows H_2CO_{3(aq)} \tag{R2}$$
$$H_2CO_{3(aq)} \rightleftarrows {HCO_3}^-{}_{(aq)} + H^+_{(aq)} \tag{R3}$$
$$MDEA_{(l)} + H^+_{(aq)} \rightleftarrows MDEAH^+_{(aq)} \tag{R4}$$

An aqueous mixture of the above mentioned chemicals will exit the absorber. This mixture is considered the "rich solvent" and will be referred to as such from this point on.

The rich solvent is moved to the stripper. In the stripper, the solvent is heated and pressurised to 378-383K and 150-200 kPa remove the acid gasses from the solvent[26]. The acid-gasses are extracted from the stripper and the regenerated solvent is moved back to the absorber. A schematic representation of the the system is presented in Figure 1.1.

The rich mixture contains the following elements: H_2O, MDEA, MDEAH+, CO_2, H_2S, HS^-, H_2CO_3, HCO_3^- and H^+. The H^+ ion is very light and contrary to the other elements, it experiences only attractive forces. For this reason, it is assumed that all H^+ ions have been absorbed into either H_3O^+ or $MDEAH^+$.

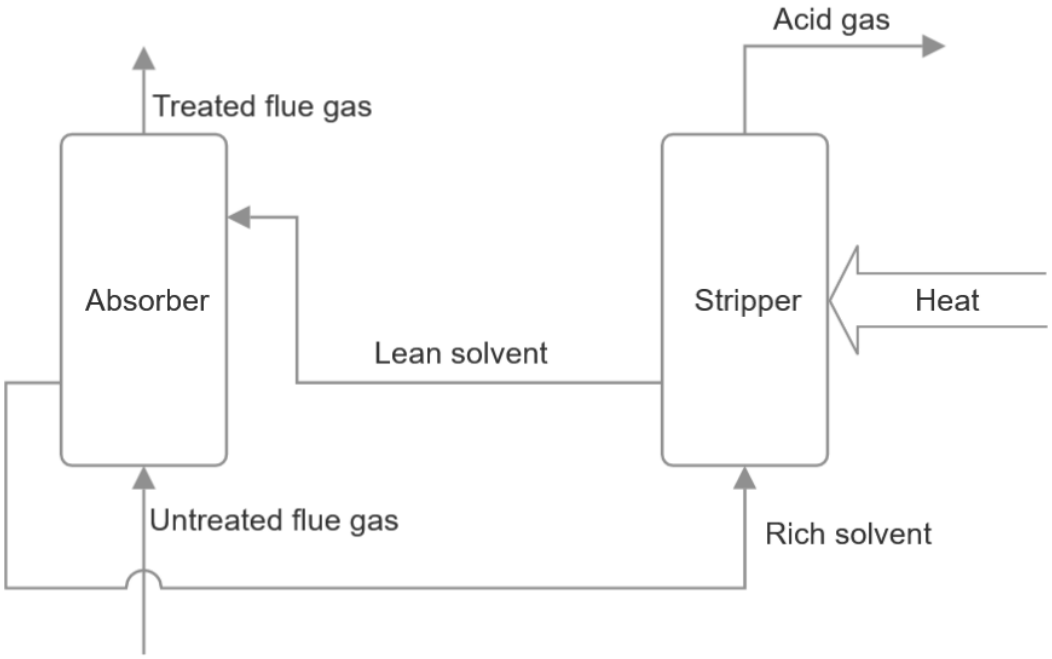

Figure 1.1: Typical acid-capture process. The lean solvent is brought into contact with the waste gas stream in the absorber, where the acid gasses to get absorbed by the solvent. The now rich solvent is moved to the strippser and heated to appproximately 378-383K to remove the acid-gasses from the solvent. The acid-gas exits the stripper, while the now regenerated solvent is returned to the absorber.

2 Methodology

2.1 Simulation Methods

The molecular dynamics (MD) simulations are conducted using LAMMPS[29]. The TIP4P/2005 force field is used for H_2O. This force field is chosen because it is known to reproduce the bulk properties of H_2O[30]. The TRAPPE[31] force field is used for CO_2, because it is a good predictor of D_{CO_2} in pure water[32]. The TRAPPE force field is used for H_2S as well. This force field comes in several variants. They are designated by the "*A*-*B*" notation, with *A* being the number of charge sites and *B* being the number of LJ sites. The difference in accuracy between the 4-3 and 3-3 variants is small[33]. Therefore, the 3-3 variant is used instead. The force field of MDEA is constructed using OPLS-AA parameters reported by Rizzo et al[34], Cornell et al[35], Jorgensen et al[36] and Orozco et al[23]. The point charges for MDEA are computed using Gaussian09[37]. These charges are scaled to obtain optimal agreement of density and viscosity with experimental data:

$$q_i^{(n)} = K_{\mathrm{e}} \cdot q_{i,100\%}^{(n)} \tag{2.1}$$

In equation 2.1, $q_{i,100\%}$ is the unscaled charge, K_{e} is the scaling factor, q_i is the charge after scaling and n is the atom number in MDEA. The atom numbers are defined in Figure 2.1d. The exact force field parameters and charges can be found in the appendix in Tables 1-6. The intermolecular LJ parameters between all species are computed using the Lorentz-Berthelot mixing rules[38], with 1 exception: the mixing rules between CO_2 and MDEA are scaled as described by equation 2.2:

$$\epsilon_{ij} = K_{\epsilon_{ij}} \cdot \sqrt{\epsilon_{ii}\epsilon_{jj}} \tag{2.2}$$

$$\sigma_{ij} = K_{\sigma_{ij}} \cdot \frac{\sigma_{ii} + \sigma_{jj}}{2} \tag{2.3}$$

With $K_{\sigma_{\mathrm{O(CO_2)O(MDEA)}}} = 0.9$ and $K_{\sigma_{\mathrm{O(CO_2)C(MDEA)}}} = 0.9$. The aim of this scaling is an increase in D_{CO_2} in a mixture of aqueous MDEA. The necessity and effect of this scaling is further elaborated on in subsections 3.1 and 3.4.1. The LJ interactions are truncated at 10 Å. The long-range coulombic interactions are computed using a particle-particle particle-mesh (pppm) solver[39] with a relative RMS error of 10^{-5}.

The initial configurations are created using the built-in "create_atoms" command of LAMMPS. The initial systems are cubic boxes with cord length $L_{\mathrm{box},0}$. The value of $L_{\mathrm{box},0}$ for each system can be found in Table 2.1. The simulations start with 2 equilibration stages of $2 \cdot 10^5$ cycles with time steps of 0.2 and 0.5 fs. Equilibration occurs in the NPT regime. Once the system is in equilibrium, the regime switches to NVT for production. The production stage is 20 ns long with a 1 fs timestep for all systems. The correct temperature and pressure are maintained at all times using a Nose-Hoover thermostat and barostat.

Viscosity and diffusivity are computed using the LAMMPS extension OCTP[40]. OCTP uses Einstein relations combined with the order-n algorithm to compute several transport properties, among which self diffusivity and bulk viscosity. Three advantages are the low computational cost, easy integration into a LAMMPS input file and the on-the-fly nature of the calculations which eliminate the need for large trajectory files[40]. The plugin is also employed to compute the radial distribution functions (RDF) in this work.

The diffusivity of species in small systems (less than 1500 molecules) may suffer from finite size effects. The method presented by Jamali et al[41] is used to correct these effects:

$$D^{\infty}_{\mathrm{i,Self}} = D^{\mathrm{MD}}_{\mathrm{i,Self}} + \frac{\xi k_b T}{6\pi\eta L} \tag{2.4}$$

In equation 2.4, ξ is a shape factor dependant on box shape ($\xi_{\mathrm{cubic}} = 2.837297$), $\mathrm{k_b}$ is the Boltzmann constant, T is the system temperature, η is the system shear viscosity and L is the box cord length.

2.2 Studied system composition

The mixing ratios that are used in simulations are based on the experimental mixtures used by Al Ghawas[16]. The total number of molecules is $N_{\mathrm{H_2O}} + N_{\mathrm{MDEA}} + N_{\mathrm{AG}} = N$, where $N_{\mathrm{H_2O}}$, N_{MDEA} and N_{AG} are the number of H_2O, MDEA and acid-gas molecules. The aqueous mixture containing 700 molecules is created first; $N_{\mathrm{H_2O}} + N_{\mathrm{MDEA}} = 700$. The number of acid gas molecules will be added afterwards; $N_{\mathrm{AG}} = 2$. The number of molecules per species and system box cord length for each simulated wt% MDEA can be found in Table 2.1. The solubility for CO_2 is given by Al Ghawas et al[16]. The solubility is used to determine the maximum number of acid gas molecules which can be inserted into the mixture. This number is calculated using the following equation;

$$N_{\mathrm{AG}} = C \cdot V \cdot N_{\mathrm{AV}} \tag{2.5}$$

where N_{AG} is the number of acid gas molecules, C is the concentration of the acid gas and N_{AV} is Avogadro's number. The resulting number of CO_2 molecules at 288K and 50wt% MDEA is 0.66. This low number would suggest only one molecule should be inserted into the mixture. Inserting more may cause phase separation due to oversaturation. The simulations in this work will still use 2 acid gas molecules in order to improve the sample size for the measurements. The systems were visualised using VMD[42]. None of the systems showed any kind of phase separation.

The rich solvent will contain dissolved CO_2 and/or H_2S. This will produce ionic molecules. The computational data is compared to data obtained using the N_2O/CO_2 analogy[16]. The N_2O molecules significantly less reactive, which means there are significantly fewer ions present in their mixture. Considering that using CO_2 yields just 1 dissociated variant of each species in the system, it is assumed that using N_2O will yield no ions in the systems studied in this work.

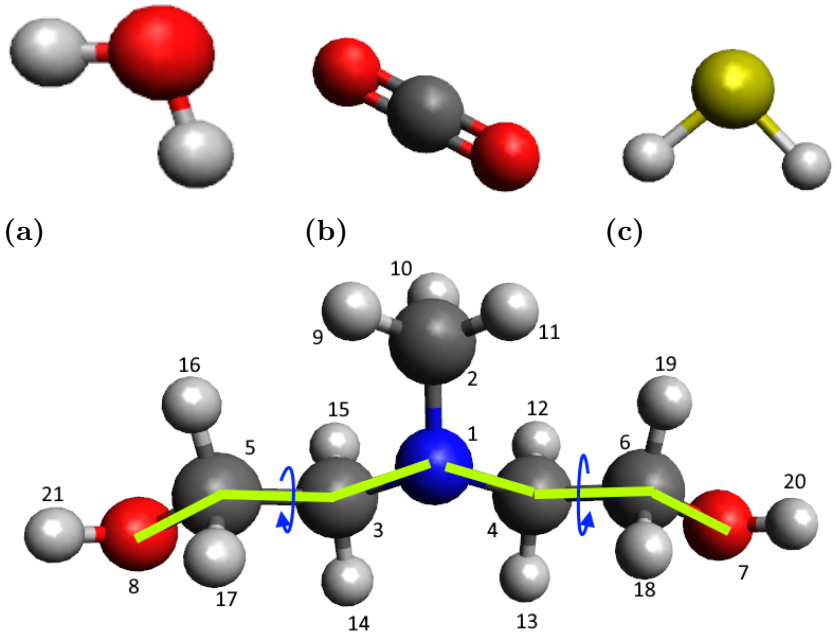

Figure 2.1: Schematic representation of H_2O(a), CO_2(b), H_2S(c) and MDEA(d). The colors blue, gray, red, white and yellow represent the nitrogen, carbon, oxygen, hydrogen and sulfur atoms, respectively. The green lines in Figure 2.1d represent the dihedral taken from Orozco et al. The atom numbering refers to the charges, which are defined in Table 6.

Table 2.1: System properties: number of molecules of each species for each wt% MDEA and the accompanying initial box size $L_{\text{box},0}$ and the size L_{box} once the volume has converged.

wt% MDEA	N_{H_2O}	N_{MDEA}	N_{AG}	$L_{\text{box},0}$[Å]	L_{box}[Å]
0	700	0	2	45	27.6
10	688	12	2	45	28.4
20	657	43	2	45	30.1
30	608	92	2	55	32.6

2.3 Validation

The force field of CO_2 is verified by computing D_{CO_2} in pure water, at the temperature extremes reported by Al Ghawas et al[16]: 288K and 323K. The resulting D_{CO_2} is compared to experimental data from Al Ghawas et al[16] and Tamimi et al[27]. The force field of H_2S is verified by computing D_{H_2S} in pure water at 3 temperatures reported by Halmour et al[43]. The results of D_{H_2S} will be compared to the experimental data reported by Halmour et al[43] and Tamimi et al[27]. The force field of MDEA is verified over 2 temperature ranges; 288-333K for density and viscosity, and 288-323K for D_{MDEA}. The viscosity will be compared to experimental data from Al Ghawas et al[16] and computational data reported by Yiannourakou et al[25]. The computed D_{MDEA} will be compared to the computational work of Yiannourakou et al[25] and experimental data from Snijder et al[44]. The temperatures used by Yiannourakou[25] do not always line up with temperatures reported by Snijder[44] and Al Ghawas[16]. Furthermore, D_{MDEA} was computed at temperatures reported by Al Ghawas[16], which do not line up with those from Snijder et al[44] either. Curves are fitted to the viscosity and D_{CO_2} from Al Ghawas[16], and D_{MDEA} from Snijder et al[44]. These curves are used to provide experimental data at a continuous temperature range at 30 wt% MDEA and 1 atm:

$$\begin{aligned} \eta_{\text{Al Ghawas}} \quad [\text{Pa}\cdot\text{s}] &= -2.217\cdot10^{-5}T^3 + 2.210\cdot10^{-2}T^2 - 7.369T + 824 \\ T_{\eta,\text{val}} &= 288 - 333K,\ R^2 = 0.999 \end{aligned} \tag{2.6}$$

$$\begin{aligned} D_{\text{MDEA, Snijder}} \quad [\text{m}^2/\text{s}] &= -2.645\cdot10^{-17}T^4 + 3.5307\cdot10^{-14}T^3 - 1.7488\cdot10^{-11}T^2 \\ &\quad +3.8285\cdot10^{-9}T - 3.1322\cdot10^{-7} \\ T_{D_{\text{MDEA}},\text{val}} &= 300 - 368K,\ R^2 = 0.999 \end{aligned} \tag{2.7}$$

$$D_{\mathrm{CO_2,Al\,Ghawas}} \quad [\mathrm{Pa \cdot s}] = 4.537 \cdot 10^{-13} T^2 - 2.276 \cdot 10^{-10} T + 2.872 \cdot 10^{-9} \tag{2.8}$$
$$T_{D_{\mathrm{CO_2}},\mathrm{val}} = 288 - 323K,\ R^2 = 0.997$$

Equations 2.6, 2.7 and 2.8 are only valid within the respective temperature ranges $T_{i,\mathrm{val}}$ of the data they are fitted to. The relative deviations will therefore only be reported if they fall in this range.

3 Results

3.1 Diffusivity of CO_2 in pure water

The aqueous CO_2 system is simulated at 288K and 323K. These particular temperatures are chosen because they are the extremes of the range reported by Al Ghawas et al[16]. The reference for bulk properties is assumed to be the same as pure TIP4P/2005 H_2O, as the mixture is infinitely dilute.

Figure 3.1 shows that the TRAPPE force field is in good agreement with the experimental data from Al Ghawas et al[16]. As mentioned before, the original TRAPPE force field in combination with MDEA produces inaccurate results for D_{CO_2}. A potential remedy is scaling the mixing rules between H_2O and CO_2. The first option is scaling $K_{\sigma_{O(H_2O)O(CO_2)}}$ down to 0.9. As shown in Figure 3.1, this does increase D_{CO_2} at both temperatures. At 288K and 323K, D_{CO_2} is respectively 37.5% and 22.5% higher than the experimental data from Al Ghawas[16]. The reduced $K_{\sigma_{O(H_2O)O(CO_2)}}$ decreases the force with which a H_2O molecule attracts CO_2 molecules for a given distance from between the two. The reduced attractive force reduces the restriction on the movement of the CO_2 molecule, which increases the mean square displacement and therefore D_{CO_2}. Scaling $K_{\epsilon_{O(H_2O)O(CO_2)}}$ to 0.9 results in a higher D_{CO_2} at high temperatures, but produces lower values at low temperatures. The reduced effectiveness can be visualized using Figure 3.2. It shows that there is not much difference between $K_{\epsilon_{O(H_2O)O(CO_2)}}$ and $K_{\sigma_{O(H_2O)O(CO_2)}}$ at $r = \sigma$. However, the reduction in magnitude is much larger at a given $r >> \sigma_0$ when scaling $K_{\sigma_{O(H_2O)O(CO_2)}}$ than when scaling $K_{\epsilon_{O(H_2O)O(CO_2)}}$.

Even though scaling $K_{\sigma_{O(H_2O)O(CO_2)}}$ does result in a larger value of D_{CO_2}, it will do so for any wt% MDEA solution. This means that it will overestimate D_{CO_2} at low wt% MDEA solutions, which causes data points which were previously correct to become inaccurate. Scaling the H_2O-CO_2 mixing rules is therefore not a suitable remedy for underestimated values of D_{CO_2}.

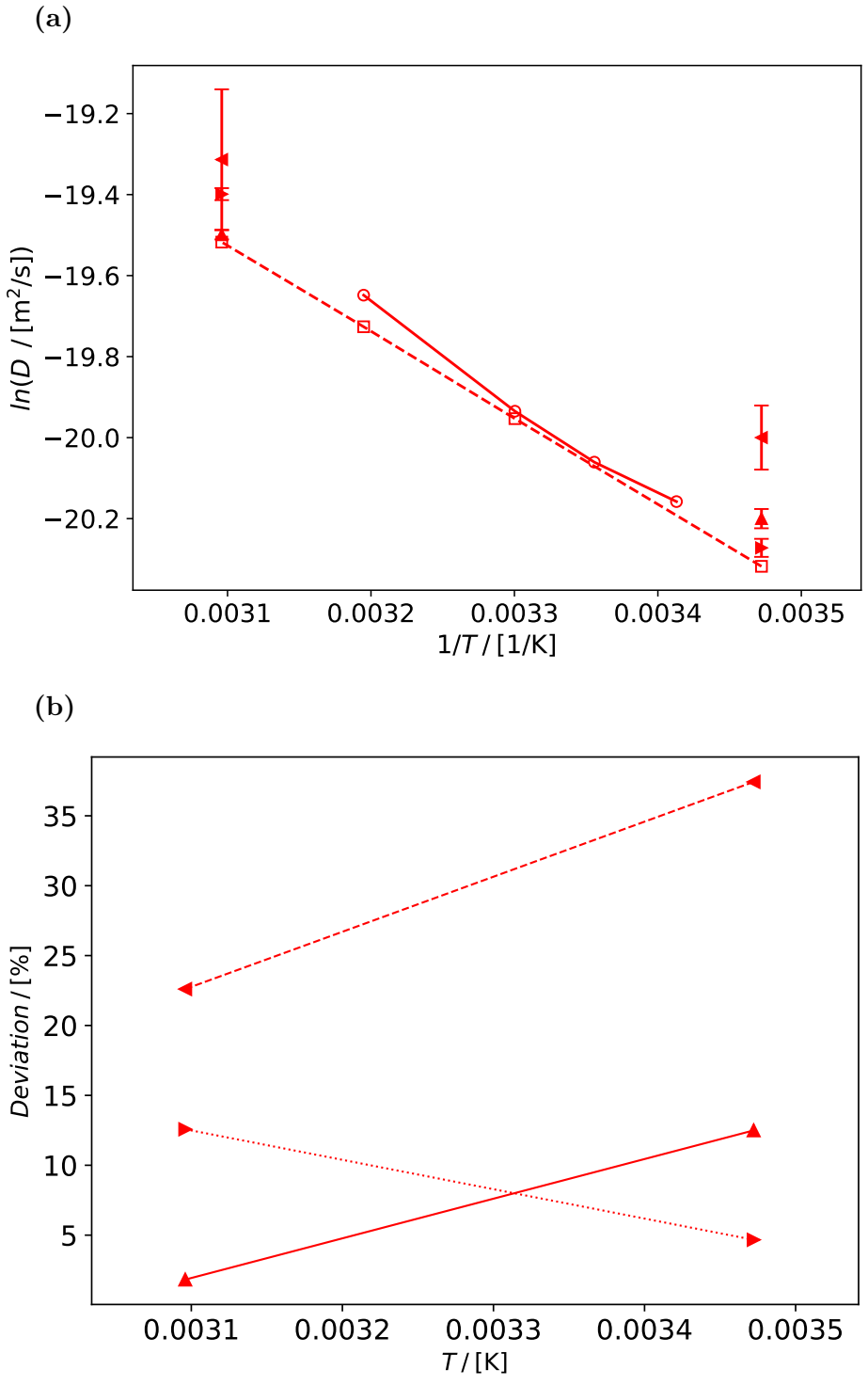

Figure 3.1: D_{CO_2} in pure water (a) and (b) its relative deviation from the data of Al Ghawas et al. The lines only serve to guide the eye. □ and ○ represent experimental data by Al Ghawas et al and Tamimi et al, respectively. TRAPPE unscaled, with scaled $K_{\sigma_{O(H_2O)O(CO_2)}}$ and scaled $K_{\epsilon_{O(H_2O)O(CO_2)}}$ are represented by ▲, ◀ and ▶, respectively.

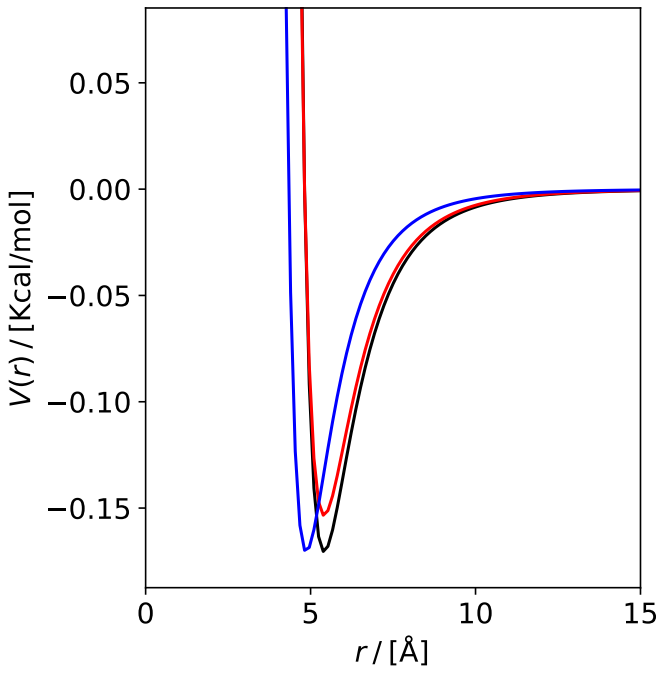

Figure 3.2: Plotted LJ mixing rules between $O(CO_2)$ and $O(H_2O)$. Unscaled, $K_{\epsilon_{O(H_2O)O(CO_2)}}$ and scaled $K_{\sigma_{O(H_2O)O(CO_2)}}$ are represented by black, red and blue, respectively.

3.2 Diffusivity of H_2S in pure water

Figure 3.3 shows that the force field is in agreement with the experimental data obtained from Halmour and Tamimi at 298K. The deviation increases to -11% and +9% at 288K and 308K, respectively.

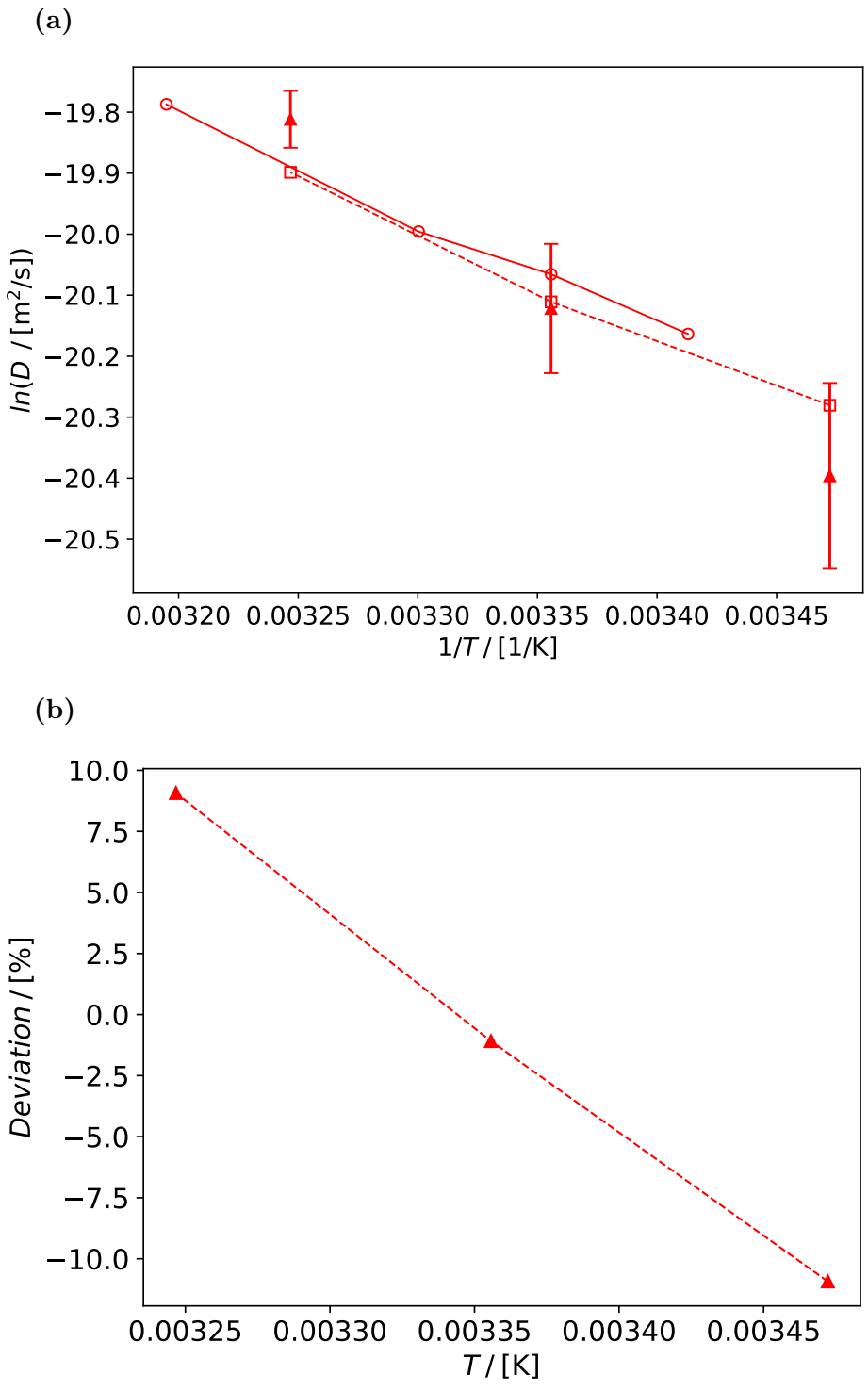

Figure 3.3: D_{H_2S} in pure water (a) and (b) its relative deviation form the data of Halmour et al. The lines only serve to guide the eye. □ and ∘ represent experimental data by Halmour et al and Tamimi et al, respectively. ▲ represents TRAPPE.

3.3 Density, viscosity and diffusivity of MDEA in pure water

The first simulations are conducted using the N-C-C-O dihedral from Cornell et al[35]. The density shown in Figure 3.5 is achieved with $K_{\mathrm{e(MDEA)}}$ scaled to 0.8. The density is accurate within 2% of the experimental data. Viscosity, shown in Figure 3.6, is up to 50% too low at 50wt% MDEA. This force field overestimates D_{MDEA} of 30wt% aqueous MDEA by approximately 200% at higher temperatures. The error becomes smaller at lower temperatures. However, the excessive error bars make this data point unreliable.

The inaccuracies for the viscosity and diffusivity increase with wt% MDEA. This suggests that the problem lies with the force field for MDEA. The physical size and stiffness of MDEA is a great influence on the viscosity. An immediate suspect is the N-C-C-O dihedral in the two alcohol groups. This dihedral is marked in Figure 2.1d. Further analysis of the visualization of the simulations shows an exceedingly flexible O-H group at the end of each alcohol group.

The dihedral is replaced by a dihedral reported by Orozco et al[23]. $K_{e(MDEA)}$ is scaled to 0.9 to achieve an optimal balance between density and viscosity. Figure 3.5, 3.6 and 3.7 respectively show the resulting density, viscosity and D_{MDEA}. The density deviation remains within 1.5% over the whole temperature range. Viscosity is now a maximum of 26% lower than experimenttal data from Al Ghawas[16]. The accuracy decreases and the standard deviation increases with decreasing temperature. The computed D_{MDEA} is in good agreement with both simulations from Yiannourakou et al[25] and experimental data from Snijder et al[44].

Figure 3.4 shows the radial distribution function of H_2O-H_2O and H_2O-MDEA for both the original dihedral from Cornell[35] and the harmonic dihedral from Orozco[23]. It shows that the effect of the new dihedral on the H_2O-H_2O interactions is negligible. The H_2O-MDEA interactions do show a small difference; the first hydration shell is slightly less populous than before. The stiffer dihedral causes the OH groups to become more resistant to deformation by the H_2O molecules, which will in turn keep the H_2O molecules further away. However, this only happens at the ends of each alcohol group. This therefore causes only a small reduction in population of the main shell, and no change in the radius of this shell.

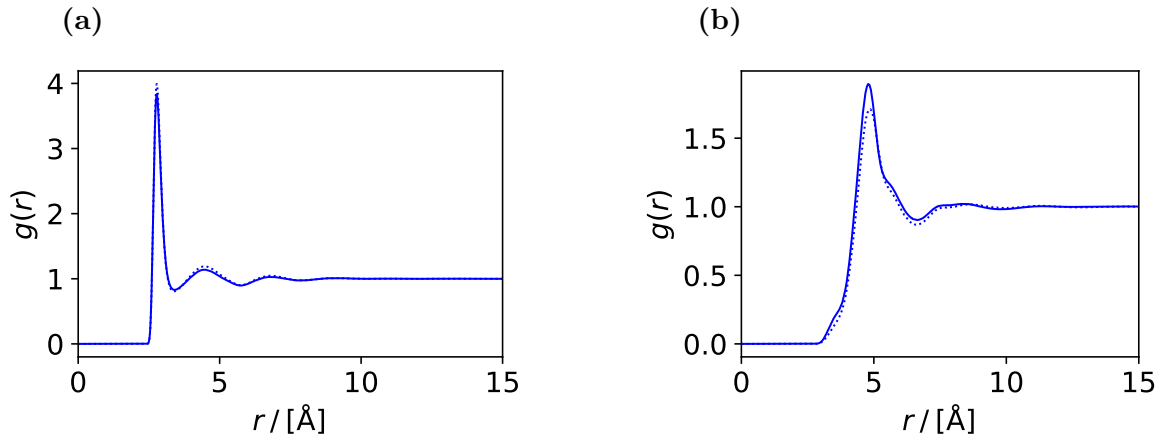

Figure 3.4: The RDF's of H_2O-H_2O (a) and (b) H_2O-MDEA molecule pairs in 30wt% aqueous MDEA at 313K and 1 atmosphere. The MDEA force field with the dihedral from Cornell et al, the dihedral from Orozco et al are represented by the continuous and dotted lines, respectively.

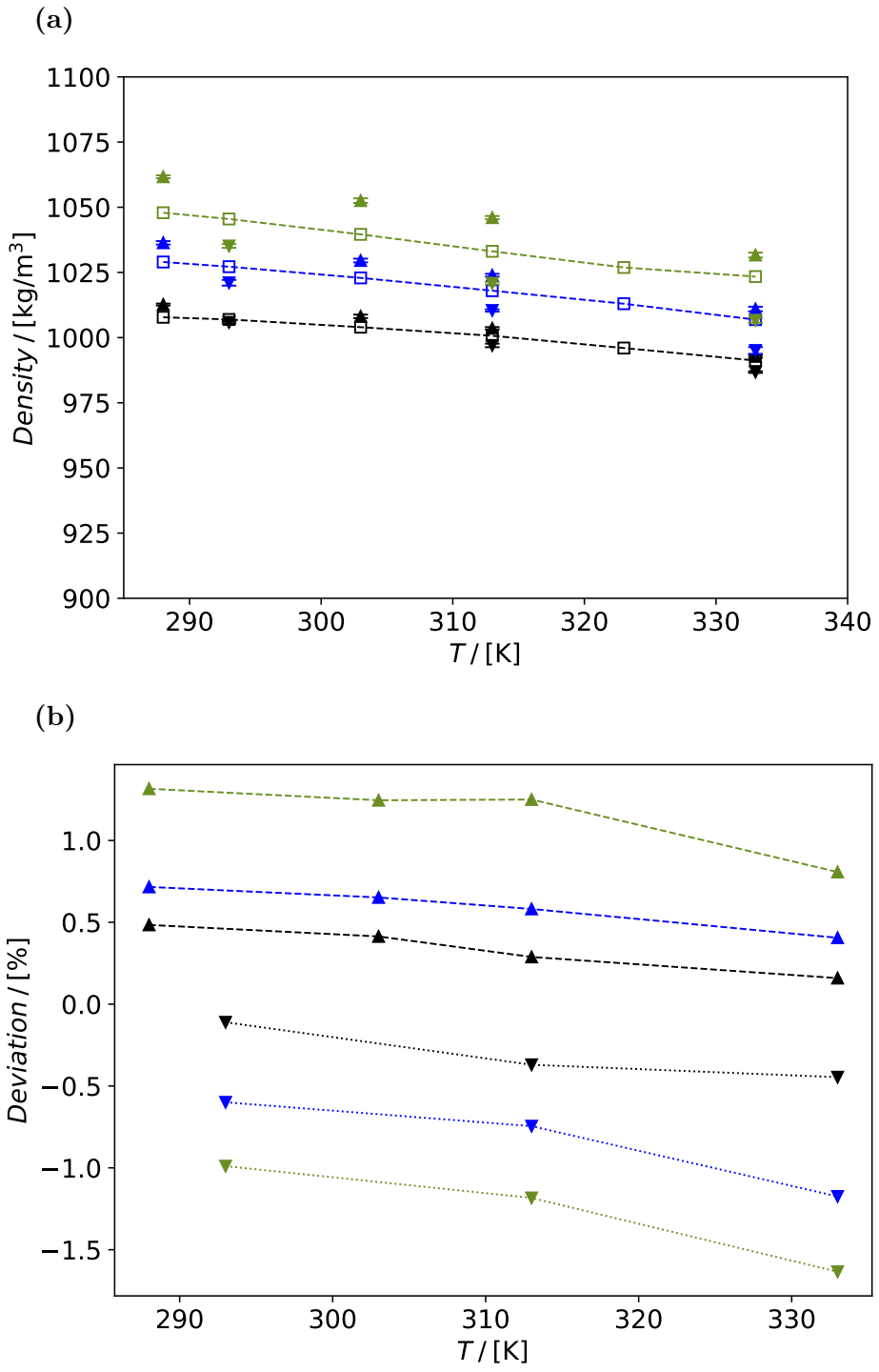

Figure 3.5: Density of aqueous MDEA (a) and (b) its relative deviation form the data of Al Ghawas et al. The lines only serve to guide the eye. Black, yellow and green represent 10, 30 and 50 wt% MDEA respectively. Experimental data from Al Ghawas et al, computational results with the N-C-C-O dihedral from Cornell et al and with the N-C-C-O dihedral from Orozco et al are represented by □, ▼ and ▲, respectively.

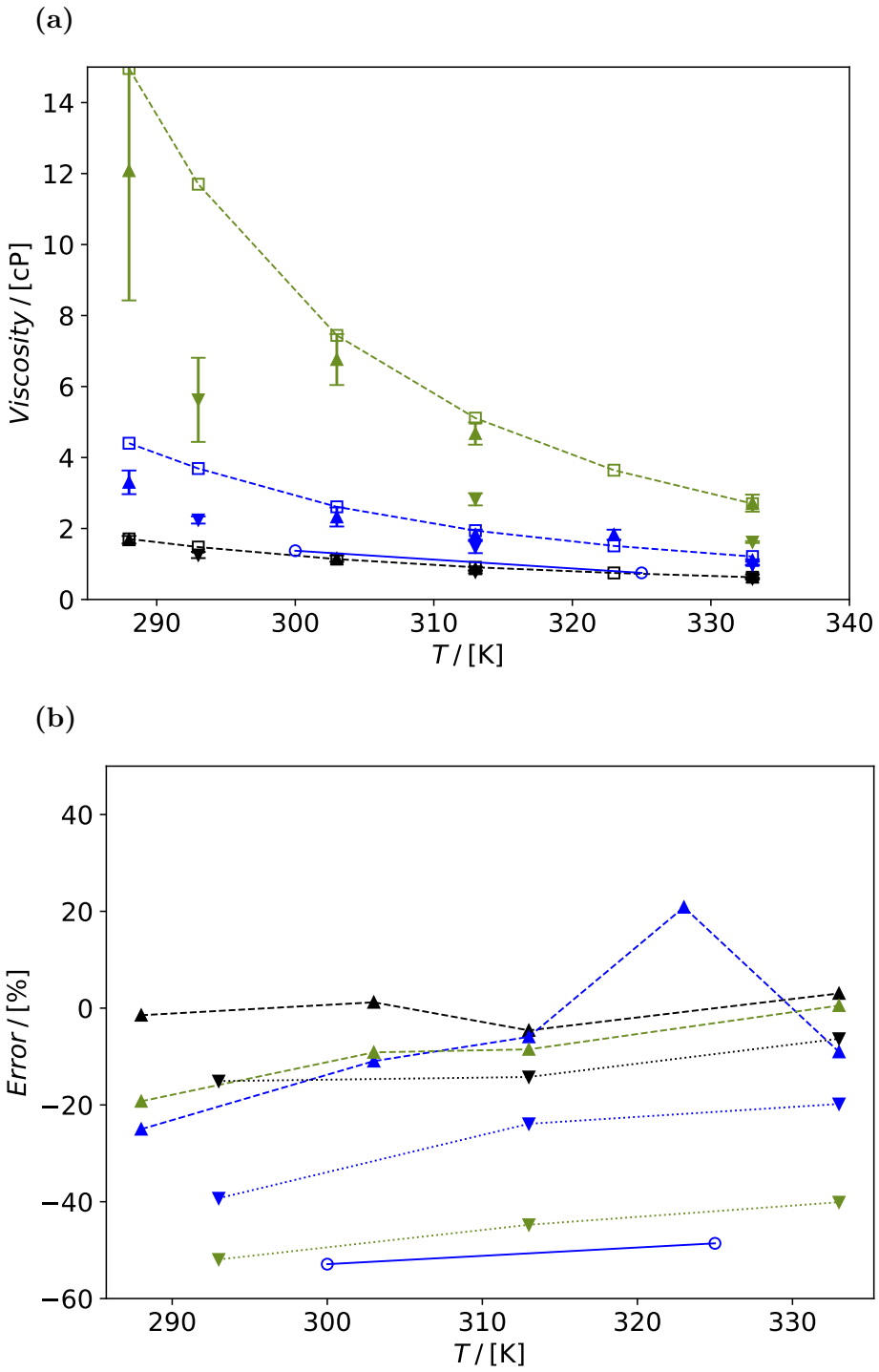

Figure 3.6: Viscosity of aqueous MDEA (a) and (b) viscosity deviation relative to data from Al Ghawas. The lines only serve to guide the eye. Black, yellow and green represent 10, 30 and 50 wt% MDEA respectively. Experimental data from Al hawas et al, computational results with the N-C-C-O dihedral from Cornell et al and with the N-C-C-O dihedral from Orozco et al are represented by □, ▼ and ▲, respectively. The computational results from Yiannourakou et al are represented by ○.

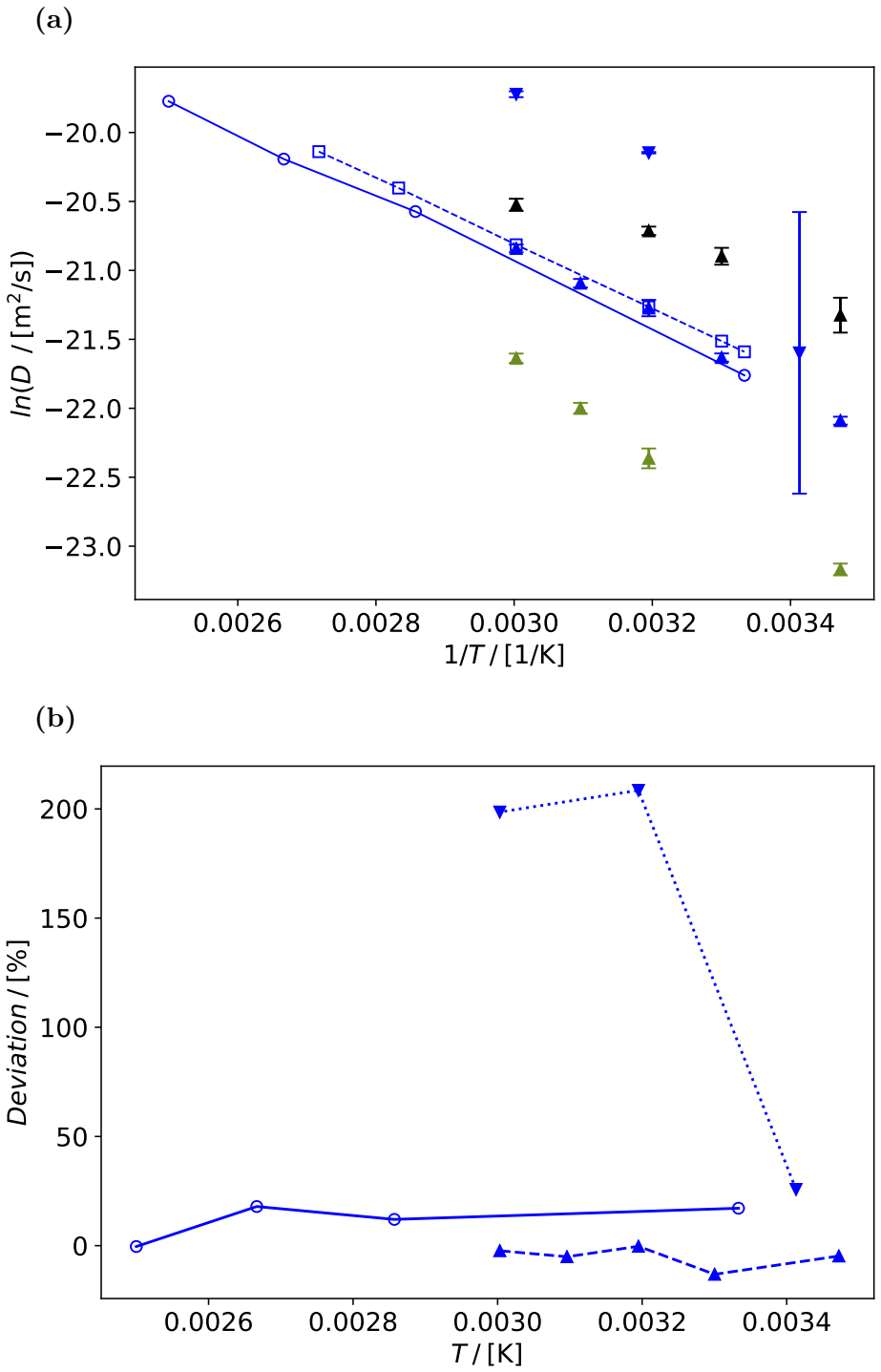

Figure 3.7: Diffusivity of MDEA in 30 wt% aqueous MDEA (a) and (b) its relative deviation form the data of Snijder et al. The lines only serve to guide the eye. Experimental data from Snijder et al, computational results with the N-C-C-O dihedral from Cornell et al and with the N-C-C-O dihedral from Orozco et al are represented by □, ▼ and ▲, respectively. The computational results from Yiannourakou et al are represented by ○.

3.4 Diffusivity of CO_2 and H_2S in aqueous MDEA

3.4.1 Diffusivity of CO_2 in aqueous MDEA

The first simulations are conducted with unmodified TRAPPE for CO_2. Figure 3.9 shows the diffusivity of CO_2 in the aqueous MDEA as a function of temperature. It shows that D_{CO_2} is underestimated at higher temperatures and higher wt% MDEA. The deviation is not a constant percentage. This can be remedied by decreasing $K_{\sigma_{\mathrm{O(CO_2)C(H_2O)}}}$ in the mixing rules between O in H_2O and the O in CO_2. As mentioned in subsection 3.1 this is moderately successful; D_{CO_2} has increased at both temperature extremes. This also means an increase in states which were accurate before the reduction of $K_{\sigma_{\mathrm{O(CO_2)O(H_2O)}}}$ as is shown in Figure 3.1. This remedy is therefore not ideal, and other options should be considered. Figure 3.9 shows that the deviation of D_{CO_2} increases in magnitude with wt% MDEA. This suggests that the source of the inaccuracies lies with the interaction between CO_2 and MDEA. The mixing rules between these two molecules are scaled. Two options are considered: $K_{\sigma_{\mathrm{O(CO_2)C(MDEA)}}}$, $K_{\sigma_{\mathrm{O(CO_2)O(MDEA)}}}$. K_ϵ will not be scaled, as Figure 3.1 shows that scaling this does not have a significant effect on D_{CO_2}. The carbon atoms are more numerous. However, $\epsilon_{\mathrm{C(MDEA)}}$ is quite small at $0.066 Kcal/mole$. There are less than half as many oxygen atoms and their LJ interactions have less reach, but $\epsilon_{\mathrm{O(MDEA)}}$ is almost 3 times as big as $\epsilon_{\mathrm{C(MDEA)}}$ at $0.170 Kcal/mole$. It is not immediately clear which interaction has a larger effect on D_{CO_2}, necessitating a simulation for both cases. The results of this are shown in Figure 3.9 as well. Scaling the individual values for K_σ has an insufficient effect. Scaling both $K_{\sigma_{\mathrm{O(CO_2)C(MDEA)}}}$ and $K_{\sigma_{\mathrm{O(CO_2)O(MDEA)}}}$ gives a small improvement. Figure 3.9b shows that the resulting values reduce the deviations by 0-5 percentage points. The reported value in this temperature range from Yiannourakou et al[25] overestimates experimental data by 80%.

Figure 3.8 shows the H_2O-CO_2 and MDEA-CO_2 rdf's. They show that the H_2O-CO_2 interactions are unchanged compared to unscaled mixing rules. This is to be expected as the mixing rules of this pair were not altered. Figure 3.8 does show a change in the interactions between MDEA and CO_2. This is caused by the reduction of $K_{\epsilon_{\mathrm{O(CO_2)\text{-}C(MDEA)}}}$ and $K_{\epsilon_{\mathrm{O(CO_2)\text{-}O(MDEA)}}}$. This reduction moves $\sigma_{\mathrm{C(MDEA)}}$ and $\sigma_{\mathrm{O(MDEA)}}$ closer to MDEA, which is visible in the fact that the entire line has moved closer to the y-axis. The peak represents the first hydration shell. The aforementioned movement of the line means this shell has reduced in radius. The peak is also lower, due to the reduced range of the LJ interactions. This reduced range reduces the chance that the attractive component pulls CO_2 to MDEA. It is again clear that the effect is relatively small.

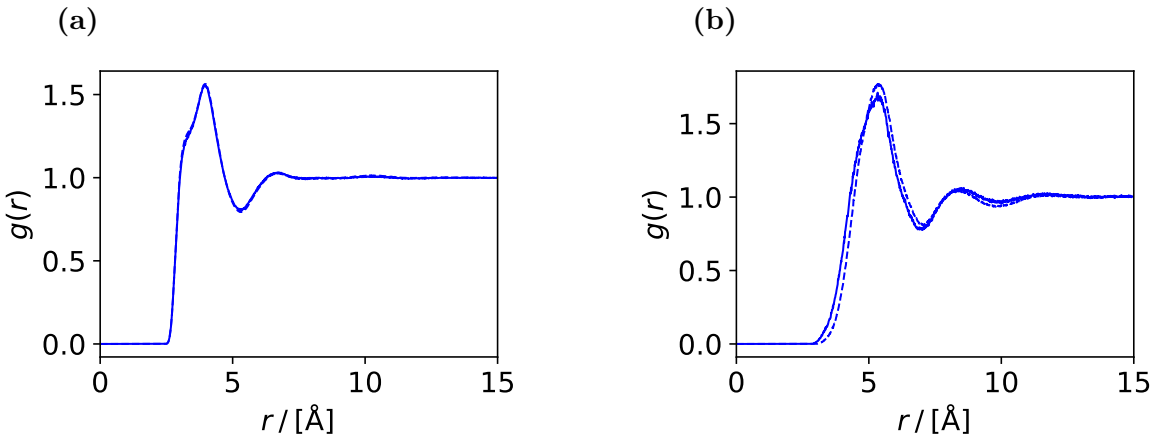

Figure 3.8: The RDF's of H_2O-CO_2 (a) and (b) MDEA-CO_2 molecule pairs in 30wt% aqueous MDEA at 313K and 1 atmosphere. The CO_2 force field with scaled mixing rules and with unscaled mixing rules are represented by the continuous and dashed lines, respectively.

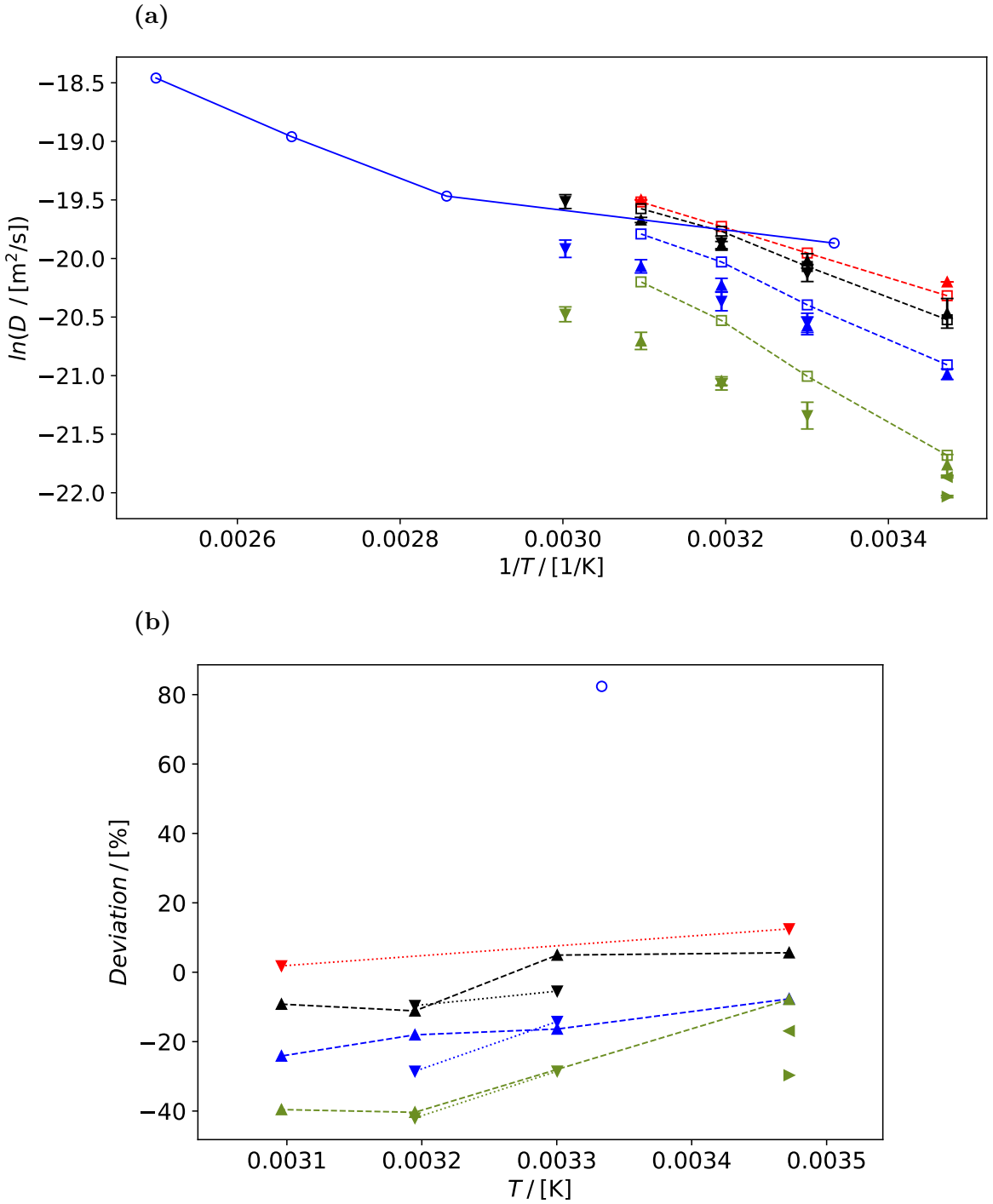

Figure 3.9: D_{CO_2} (a) and (b) its deviation relative to data from Al Ghawas. The lines only serve to guide the eye. Red, black, yellow and green represent 0, 10, 30 and 50 wt% MDEA. Experimental data from Al Ghawas et al, computational results with unscaled and scaled mixing rules are represented by □, ▼ and ▲, respectively. The results with just $K_{\sigma O(CO_2)\text{-}O(MDEA)}$ or just $K_{\sigma O(CO_2)\text{-}C(MDEA)}$ scaled to 0.9 are represented by ◄ and ►, respectively. The computational results from Yiannourakou et al are represented by ○.

3.4.2 Diffusivity of H_2S in aqueous MDEA

Figure 3.10 shows the results of D_{H_2S}. The relationship between D_{H_2S} and wt% MDEA shows the expected behavior; an increase in wt% MDEA gives a decrease in D_{H_2S}. Deviations from experimental data are only known for 0 wt% MDEA i.e. pure water. These can be found in Figure 3.3b.

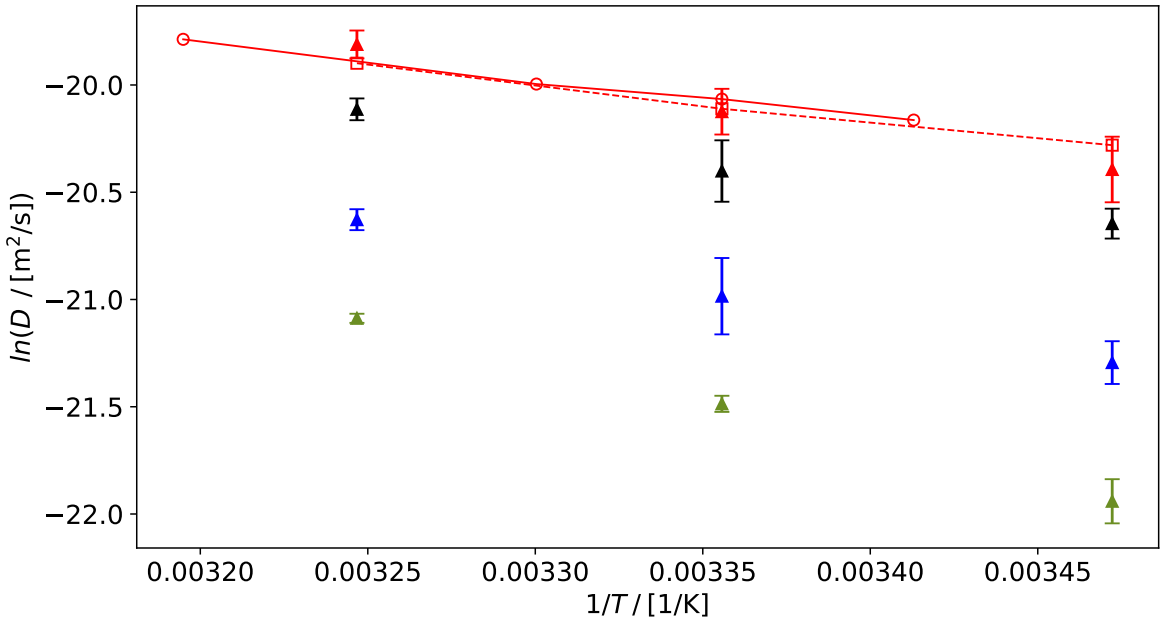

Figure 3.10: D_{H_2S}. Red, black, blue and green represent 0, 10, 30 and 50 wt% MDEA. The lines only serve to guide the eye. □ and ○ represent experimental data by Hamour et al and Tamimi et al, respectively. ▲ represents computational results with MDEA using the N-C-C-O dihedral from Orozco et al.

4 Conclusions

The purpose of this work was to investigate the transport properties of acid gasses in aqueous MDEA and fill the gap in literature. Furthermore, the force field of MDEA will give improved computational results for bulk properties, primarily viscosity, of aqueous MDEA solvents. The properties obtained in this work will aid in the design of new reactors employing aqueous MDEA solvents. The transport properties are a significant challenge to measure experimentally. A system was created with H_2O and MDEA to obtain the density, viscosity and D_{MDEA} of aqueous MDEA. Acid-gasses were added, either CO_2 or H_2S compute their diffusivity; $D_{\mathrm{CO_2}}$ or $D_{\mathrm{H_2S}}$. Reactions and ions were omitted as we were comparing to experimental data which uses the N_2O analogy, which is a molecule which will not react with this mixture. These results are therefore applicable to free CO_2.

Density was reproduced with a maximum 2% deviation from experimental values. This force field can be used for densities of aqueous mixtures of up to 50 wt% MDEA. The computed viscosity is very close to experimental data for temperatures in the 303-333K range. It can therefore be used to obtain viscosity in this range in mixtures up to 50 wt%. The deviation becomes smaller at higher temperatures, which means that it is likely to be accurate at temperatures higher than the range presented in this work.

The diffusivities of MDEA, CO_2 and H_2S were computed as well. The computed results of D_{MDEA} were within 10% of experimental values over the entire range of temperatures. It is underestimated by a relatively consistent percentage, which implies that a correction factor could be employed to obtain 1-to-1 accurate results. The computed diffusivity of CO_2 was initially underestimated when employing the unchanged TRAPPE force field for CO_2. The mixing rules between MDEA and CO_2 were scaled improve results. The final results of $D_{\mathrm{CO_2}}$ are within 11% of experimental data for 0-10 wt% MDEA across the entire range of 288-333K. The deviation is within 15% for the whole range of 0-50 wt% at 288K. Accuracy reduces at higher wt%'s MDEA and higher temperatures. No literature was found reporting $D_{\mathrm{H_2S}}$ in aqueous MDEA. The computed results do show the expected ordering: $D_{\mathrm{H_2S}}$ decreases with both temperature and increasing wt% MDEA.

4.1 Recommendations

The final force field of MDEA produces less accurate results for viscosity for temperatures lower than 303K. Furthermore, it was not verified in its pure form, as it was not the focus of this research. More research can be conducted to improve bulk property behavior at lower temperatures and at more than 50 wt% MDEA. The computed results of $D_{\mathrm{CO_2}}$ underestimate experimental results. The mixing rules between MDEA and CO_2 were adjust to achieve better results. Further research can be conducted to raise $D_{\mathrm{CO_2}}$ further. This will again likely involve

the force field of MDEA, due to the error increasing with the mass fraction of MDEA. Involving ions may influence the behavior. However, the system of 700 molecules would only be able to dissolve 1 molecule of CO_2. This would therefore only create one molecule of HCO_3^- and one $MDEAH^+$. Some research is necessary, as it is not obvious whether the effect of such a small number of ions is negligible. Literature reporting solubility of acid gasses in aqueous MDEA is equally as scarce as that of D_{CO_2}. This property is important in the acid gas capture process as it determines how much the solvent can process. Reaction force fields can be employed to study the influence of reactions on the diffusivity of both acid gasses. This may prove difficult to verify as measuring diffusivity when the gas reacts with the solvent very difficult.

No literature was found reporting D_{H_2S} in aqeuous MDEA. The presented computed results require verification which only experimental data can provide.

Appendix

Atom type	Atom	ϵ [kcal/mol]	σ [Å]	q [e$^-$]	Source
OH	O(H_2O)	0.1852	3.1589	−1.1128	Abascal[45]
HO	H(H_2O)	0	0	0.5564	Abascal[45]
CO	C(CO_2)	0.0536515	2.8	0.7	Potoff[31]
OC	O(CO_2)	0.157	3.05	−0.35	Potoff[31]
SH	S(H_2S)	0.2486	3.6	−0.28	Shah[33]
HS	H(H_2S)	0.09945	2.5	0.14	Shah[33]
NT	N(MDEA)	0.170	3.3	–	Rizzo[34]
CT(NT)	C(MDEA)	0.030	2.5	–	Rizzo[34]
OH	O(MDEA)	0.170	3.12	–	Jorgensen[36]
HC(CT)	H(MDEA)	0.030	2.5	–	Rizzo[34]
HC(Alkanes)	H(MDEA)	0.015	2.5	–	Rizzo[34]
HO	H(MDEA)	0.001	1	–	-

Table 1: OPLS-AA Non-Bonded Parameters

Bond	Molecule	k_b [kcal mol^{-1} Å^{-2}]	r_0 [Å]	Source
O-H	H_2O	rigid	0.9572	Abascal[45]
C-O	CO_2	rigid	1.16	Potoff[31]
S-H	H_2S	rigid	1.34	Shah[33]
CT(NT)-CT(NT)	MDEA	268	1.529	Rizzo[34]
CT(NT)-NT	MDEA	382	1.448	Rizzo[34]
CT(NT)-OH	MDEA	320	1.41	Cornell[35]
CT(NT)-HC(CT)	MDEA	340	1.09	Rizzo[34]
CT(NT)-HC	MDEA	340	1.09	Rizzo[34]
OH-HO	MDEA	553	0.96	Cornell[35]

Table 2: OPLS-AA Bond Stretching Parameters

Bond	Molecule	k_b [kcal mol^{-1} deg^{-2}]	r_0 [deg]	Source
H-O-H	H_2O	rigid	104.52	Abascal[45]
C-C-O	CO_2	rigid	180	Potoff[31]
H-S-H	H_2S	rigid	92	Shah[33]
CT(NT)-CT(NT)-NT	MDEA	56.2	107.2	Rizzo[34]
CT(NT)-NT-CT(NT)	MDEA	51.8	107.2	Rizzo[34]
CT(NT)-CT(NT)-HC	MDEA	37.5	110.7	Rizzo[34]
HC-CT-HC	MDEA	33	107.8	Rizzo[34]
CT(NT)-CT(NT)-OH	MDEA	50	109.5	Cornell[35]
CT(NT)-OH-HO	MDEA	55	108.5	Cornell[35]
HC-CT(NT)-OH	MDEA	50	109.5	Cornell[35]

Table 3: OPLS-AA Angle Stretching Parameters

Dihedral angle	V_1	V_2	V_3	V_4	Source
HC(CT)-CT(NT)-NT-CT(NT)	0.0	0.0	0.56	0.0	Rizzo[34]
CT(CT)-NT-CT(NT)-CT(NT)	0.416	−0.128	0.695	0.0	Rizzo[34]
CT(NT)-CT(NT)-OH-HO	−0.356	−0.174	0.492	0.0	Jorgensen[36]

Table 4: OPLS-AA Dihedral Parameters

Dihedral angle	NT-CT(NT)-CT(NT)-OH
V_1	0.11326434
V_2	0.70396196
V_3	2.446330913
V_4	-18.73628653
V_5	-13.08348189
V_6	28.94651043
V_7	13.14424721
V_8	-22.54397533
V_9	4.989989675

Table 5: Harmonic Dihedral Parameters from Orozco et al [Kcal/mol]

Atom nr	q[e]
1	−0.571725
2	−0.23472
3	−0.098037
4	−0.102465
5	0.058014
6	0.062748
7	−0.703863
8	−0.699813
9	0.151056
10	0.146421
11	0.128142
12	0.156429
13	0.137115
14	0.15741
15	0.12735
16	0.116946
17	0.11088
18	0.116109
19	0.10917
20	0.416034
21	0.416799

Table 6: Atom-by-atom charges of MDEA, numbering adheres to Figure 2.1d

Bibliography

[1] R. K. Pachauri, M. R. Allen, V. R. Barros, J. Broome, W. Cramer, R. Christ, J. A. Church, L. Clarke, Q. Dahe, P. Dasgupta, N. K. Dubash, O. Edenhofer, I. Elgizouli, C. B. Field, P. Forster, P. Friedlingstein, J. Fuglestvedt, L. Gomez-Echeverri, S. Hallegatte, G. Hegerl, M. Howden, K. Jiang, B. Jimenez Cisneroz, V. Kattsov, H. Lee, K. J. Mach, J. Marotzke, M. D. Mastrandrea, L. Meyer, J. Minx, Y. Mulugetta, K. O'Brien, M. Oppenheimer, J. J. Pereira, R. Pichs-Madruga, G.-K. Plattner, Hans-Otto Pörtner, S. B. Power, B. Preston, N. H. Ravindranath, A. Reisinger, K. Riahi, M. Rusticucci, R. Scholes, K. Seyboth, Y. Sokona, R. Stavins, T. F. Stocker, P. Tschakert, D. van Vuuren, and J.-P. van Ypserle. Climate Change 2014: Synthesis Report. Contribution of Working Groups I, II and III to the Fifth Assessment Report of the Intergovernmental Panel on Climate Change. IPCC, Geneva, Switzerland, 2014.

[2] V. Masson-Delmotte, P. Zhai, H. Portner, D. Roberts, J. Skea, P. R. Shukla, A. Pirani, W. Moufouma-Okia, C. Pe, R. Pidcock, S. Connors, J. B. R. Matthews, Y. Chen, X. Zhou, M. I. Gomis, E. Lonnoy, T. Maycock, M. Tignor, and T. Waterfield. Global Warming of 1.5 °C. An IPCC Special Report on the impacts of global warming of 1.5°C above pre-industrial levels and related global greenhouse gas emission pathways, in the context of strengthening the global response to the threat of climate change. IPCC, Geneva, Switzerland, 2018.

[3] M.Wang, A. Lawal, P.Stephenson, J. Sidders, and C. Ramshaw. Post-combustion co2 capture with chemical absorption: A state-of-the-art review. Chemical engineering research and design, 89(9):1609–1624, 2011.

[4] Seyed Mohsen Hosseini-Ardali, Majid Hazrati-Kalbibaki, and Ferenc Lezsovits Moslem Fattahi. Multi-objective optimization of post combustion co2 capture using methyldiethanolamine (mdea) and piperazine (pz) bi-solvent. Energy, 211, 2020.

[5] Juliana G.M.-S. Monteiro, Diego D.D. Pinto, Syed A.H. Zaidy, Ardi Hartono, and Hallvard F. Svendsen. Vle data and modelling of aqueous n,n-diethylethanolamine (deea) solutions. International Journal of Greenhouse Gas Control, 19:432–440, 2013.

[6] Patricia Luis. Use of monoethanolamine (mea) for co2 capture in a global scenario: Consequences and alternatives. Desalination, 380:93–99, 2016.

[7] Ugochukwu E. Aronu, Shahla Gondal, Erik T. Hessen, Tore Haug-Warberg, Ardi Hartono, Karl A. Hoff, and Hallvard F. Svendsen. Solubility of co2 in 15, 30, 45 and 60 mass% mea from 40 to 120°c and model representation using the extended uniquac framework. Chemical Engineering Science, 66(24):6393–6406, 2011. Novel Gas Conversion Symposium-Lyon 2010, C1-C4 Catalytic Processes for the Production of Chemicals and Fuels.

[8] Noorlisa Harun, Thanita Nittaya, Peter L. Douglas, Eric Croiset, and Luis A. Ricardez-Sandoval. Dynamic simulation of mea absorption process for co2 capture from power plants. International Journal of Greenhouse Gas Control, 10:295–309, 2012.

[9] J. Kittel, R. Idem, D. Gelowitz, P. Tontiwachwuthikul, G. Parrain, and A. Bonneau. Corrosion in mea units for co2 capture: Pilot plant studies. Energy Procedia, 1(1):791–797, 2009. Greenhouse Gas Control Technologies 9.

[10] Se-Young Oh, Michael Binns, Habin Cho, and Jin-Kuk Kim. Energy minimization of mea-based co2 capture process. Applied Energy, 169:353–362, 2016.

[11] H. Mert Polat, Frédérick de Meyer, Céline Houriez, Christophe Coquelet, Othonas A. Moultos, and Thijs J.H. Vlugt. Transport properties of mixtures of acid gases with aqueous monoethanolamine solutions: A molecular dynamics study. Fluid Phase Equilibria, 564:113587, 2023.

[12] Eirik F. da Silva, Tatyana Kuznetsova, Bjørn Kvamme, and Kenneth M. Merz. Molecular dynamics study of ethanolamine as a pure liquid and in aqueous solution. The Journal of Physical Chemistry B, 111(14):3695–3703, 2007. PMID: 17388544.

[13] J. K. A. Clarke. Kinetics of absorption of cardon dioxide in monoethanolamine solutions at short contact times. Industrial & Engineering Chemistry Fundamentals, 3(3):239–245, 1964.

[14] A. Tamimi, E. B. Rinker, and O. C. Sandall. Diffusivity of nitrous oxide in aqueous solutions of methyldiethanolamine and diethanolamine from 293 to 368 k. Journal of chemical engineering data, 39(2):396–398, 1994.

[15] Jiun-Jie Ko, Tung-Chien Tsai, Chih-Yuan Lin, Hsiun-Min Wang, and Meng-Hui Li. Diffusivity of nitrous oxide in aqueous alkanolamine solutions. Journal of Chemical & Engineering Data, 46(1):160–165, 2001.

[16] Hani A. Al-Ghawas, Daniel P. Hagewiesche, Gabriel Ruiz-Ibanez, , and Orville C. Sandall. Physiochemical properties important for carbon dioxide absorption in aqueous methyldiethanolamine. Journal of chemical engineering data, 34(4):385–391, 1989.

[17] Anne Penttilä, Claudia Dell'Era, Petri Uusi-Kyyny, and Ville Alopaeus. The henry's law constant of n2o and co2 in aqueous binary and ternary amine solutions (mea, dea, dipa, mdea, and amp). Fluid Phase Equilibria, 311:59–66, 2011.

[18] Qu Chen, Sayee Prasaad Balaji, Mahinder Ramdin, Juan José Gutiérrez-Sevillano, André Bardow, Earl Goetheer, and Thijs J. H. Vlugt. Validation of the co2/n2o analogy using molecular simulation. Industrial & Engineering Chemistry Research, 53(46):18081–18090, 2014.

[19] V. Lachet, B. Creton, T. de Bruin, E. Bourasseau, N. Desbiens, O. Wilhelmsen, and M. Hammer. Equilibrium and transport properties of co2+n2o and co2+no mixtures: Molecular simulation and equation of state modelling study. Fluid Phase Equilibria, 322-323:66–78, 2012.

[20] Tjoon T Teng, Yadollah Maham, Loren G Hepler, and Alan E Mather. Viscosity of aqueous solutions of n-methyldiethanolamine and of diethanolamine. Journal of Chemical and Engineering Data, 39(2):290–293, 1994.

[21] R. Yusoff, M. K. Aroua, Ahmad Shamiri, Afshin Ahmady, N. S. Jusoh, N. F. Asmuni, L. C. Bong, and S. H. Thee. Density and viscosity of aqueous mixtures of n-methyldiethanolamines (mdea) and ionic liquids. Journal of Chemical & Engineering Data, 58(2):240–247, 2013.

[22] Eduardo I. Concepción, Alejandro Moreau, M. Carmen Martín, David Vega-Maza, and José J. Segovia. Density and viscosity of aqueous solutions of methyldiethanolamine (mdea) + diethanolamine (dea) at high pressures. The Journal of Chemical Thermodynamics, 148:106141, 2020.

[23] Gustavo A. Orozco, Véronique Lachet, Carlos Nieto-Draghi, and Allan D. Mackie. A transferable force field for primary, secondary, and tertiary alkanolamines. Journal of Chemical Theory and Computation, 9(4):2097–2103, 2013.

[24] Y. S. Yu, H. F. Lu, G. X. Wang, Z. X. Zhang, and V. Rudolph. Characterizing the transport properties of multiamine solutions for co2 capture by molecular dynamics simulation. Journal of chemical and engineering data, 58(6):1429–1439, 2013.

[25] Marianna Yiannourakou, Xavier Rozanska, Benoit Minisini, and Frédérick de Meyer. Molecular simulations for improved process modeling of an acid gas removal unit. Fluid Phase Equilibria, 560:113478, 2022.

[26] Sumedh S. Warudkar, Kenneth R. Cox, Michael S. Wong, and George J. Hirasaki. Influence of stripper operating parameters on the performance of amine absorption systems for post-combustion carbon capture: Part i. high pressure strippers. International Journal of Greenhouse Gas Control, 16:342–350, 2013.

[27] A. Tamimi, E. B. Rinker, and O. C. Sandall. Diffusion coefficients for hydrogen sulfide, carbon dioxide, and nitrous oxide in water over the temperature range 293-368 k. Journal of chemical engineering data, 39(2):330–332, 1994.

[28] J. Kittel, E. Fleury, S. Gonzalez, and Ropital Francois. Acid gas removal by amine solvents : bridges between co 2 capture and natural gas treatment. 2020.

[29] A. P. Thompson, H. M. Aktulga, R. Berger, D. S. Bolintineanu, W. M. Brown, P. S. Crozier, P. J. in 't Veld, A. Kohlmeyer, S. G. Moore, T. D. Nguyen, R. Shan, M. J. Stevens, J. Tranchida, C. Trott, and S. J. Plimpton. LAMMPS - a flexible simulation tool for particle-based materials modeling at the atomic, meso, and continuum scales. Comp. Phys. Comm., 271:108171, 2022.

[30] Carlos Vega and Jose L. F. Abascal. Simulating water with rigid non-polarizable models: a general perspective. Phys. Chem. Chem. Phys., 13:19663–19688, 2011.

[31] Jeffrey J. Potoff and J. Ilja Siepmann. Vapor-liquid equilibria of mixtures containing alkanes, carbon dioxide, and nitrogen. AIChE Journal, 47(7):1676–1682, 2001.

[32] Othonas A. Moultos, Ioannis N. Tsimpanogiannis, Athanassios Z. Panagiotopoulos, and Ioannis G. Economou. Atomistic molecular dynamics simulations of co2 diffusivity in h2o for a wide range of temperatures and pressures. The journal of physical chemistry B, 118:5532–5541, 2014.

[33] Mansi S. Shah, Michael Tsapatsis, and J. Ilja Siepmann. Development of the transferable potentials for phase equilibria model for hydrogen sulfide. Journal of physical chemistry B, 119(23):7041–7052, 2015.

[34] Robert C. Rizzo and William L. Jorgensen. Opls all-atom model for amines: Resolution of the amine hydration problem. Journal of the American Chemical Society, 121(20):4827–4836, 1999.

[35] Wendy D. Cornell, Piotr Cieplak, Christopher I. Bayly, Ian R. Gould, Kenneth M. Merz, David M. Ferguson, David C. Spellmeyer, Thomas Fox, James W. Caldwell, and Peter A. Kollman. A second generation force field for the simulation of proteins, nucleic acids, and organic molecules. Journal of the American Chemical Society, 117(19):5179–5197, 1995.

[36] William L. Jorgensen, David S. Maxwell, and Julian Tirado-Rives. Development and testing of the opls all-atom force field on conformational energetics and properties of organic liquids. Journal of the American Chemical Society, 118(45):11225–11236, 1996.

[37] M. J. Frisch, G. W. Trucks, H. B. Schlegel, G. E. Scuseria, M. A. Robb, J. R. Cheeseman, G. Scalmani, V. Barone, G. A. Petersson, H. Nakatsuji, X. Li, M. Caricato, A. Marenich, J. Bloino, B. G. Janesko, R. Gomperts, B. Mennucci, H. P. Hratchian, J. V. Ortiz, A. F. Izmaylov, J. L. Sonnenberg, D. Williams-Young, F. Ding, F. Lipparini, F. Egidi, J. Goings, B. Peng, A. Petrone, T. Henderson, D. Ranasinghe, V. G. Zakrzewski, J. Gao, N. Rega, G. Zheng, W. Liang, M. Hada, M. Ehara, K. Toyota, R. Fukuda, J. Hasegawa, M. Ishida, T. Nakajima, Y. Honda, O. Kitao, H. Nakai, T. Vreven, K. Throssell, J. A. Montgomery, Jr., J. E. Peralta, F. Ogliaro, M. Bearpark, J. J. Heyd, E. Brothers, K. N. Kudin, V. N. Staroverov, T. Keith, R. Kobayashi, J. Normand, K. Raghavachari, A. Rendell, J. C. Burant, S. S. Iyengar, J. Tomasi, M. Cossi, J. M. Millam, M. Klene, C. Adamo, R. Cammi, J. W. Ochterski, R. L. Martin, K. Morokuma, O. Farkas, J. B. Foresman, , and D. J. Fox. Gaussian˜09 Revision A.02, 2016. Gaussian Inc. Wallingford CT.

[38] M.P. Allen and D.J. Tildesley. Computer Simulation of Liquids. OUP Oxford, 2017.

[39] R. W. Hockney and J. W. Eastwood. Computer simulation using particles. Bristol: Hilger, 1988, 1988.

[40] Seyed Hossein Jamali, Ludger Wolff, Tim M. Becker, Mariette de Groen, Mahinder Ramdin, Remco Hartkamp, Andre Bardo, Thijs J. H. Vlug, , and Othonas A. Moultos. Octp: A tool for on-the-fly calculation of transport properties of fluids with the order-n algorithm in lammps. Journal of chemical information and modelling, 59(4):1290–1294, 2019.

[41] Seyed Hossein Jamali, André Bardow, Thijs J. H. Vlugt, and Othonas A. Moultos. Generalized form for finite-size corrections in mutual diffusion coefficients of multicomponent mixtures obtained from equilibrium molecular dynamics simulation. Journal of Chemical Theory and Computation, 16(6):3799–3806, 2020. PMID: 32338889.

[42] William Humphrey, Andrew Dalke, and Klaus Schulten. VMD – Visual Molecular Dynamics. Journal of Molecular Graphics, 14:33–38, 1996.

[43] Noman Halmour and Orville C. Sandall. Molecular diffusivity of hydrogen sulfide in water. Journal of Chemical and Engineering Data, 29(1):20–22, 1984.

[44] Erwin D. Snijder, Marcel J. M. te Riele, Geert F. Versteeg, and W. P. M. van Swaaij. Diffusion coefficients of several aqueous alkanolamine solutions. Journal of Chemical & Engineering Data, 38(3):475–480, 1993.

[45] J. Abascal and C. Vega. A general purpose model for the condensed phases of water: Tip4p/2005. Journal of chemical physics, 123, 2005.